Chapter 5

The lift-off process of CVD-grown $CuGaSe_2$

A field of increasing technological and scientific interest in photovoltaics is the processing of thin-film solar cells on alternative substrates, where *alternative* is in this context understood as a substrate material other than conventional glass or a piece of wafer, and which may indeed show interesting properties (e.g. lightness or flexibility) for specific applications. A number of contributions on the topic can be found in the proceedings of international conferences and workshops during the last years (some of which will be referenced in the following), facing the problem from different perspectives. Generally speaking, two main approaches are currently accepted:

- The direct growth of the active layer on the alternative substrate. This option is economically convenient but it is in turn constrained to alternative substrates able to withstand the working conditions of a given processing chamber, in particular those of high temperatures and possibly a highly reactive chemical environment. This approach is therefore normally limited to the use of substrates such as ceramics[211] or flexible metal foils[212, 213], not being suitable for plastic and organic materials.

- The transfer of the thin-film absorber layer grown on a standard primary substrate to an alternative substrate with the desired features, e. g. flexibility, lightness, etc. This approach requires longer processing times and the use of two substrates, even though the primary substrate might be recyclable for further processing. On the other hand, this method relaxes the limitations imposed regarding hardness and inertness of the alternative substrates for direct processing, as long as the critical processing conditions are effective on the primary substrate, opening the possibility of implementing photovoltaic devices on soft and economic materials (e. g. organic or plastic foils) as end-products.

The appealing possibility of product commercialisation based on economic substrates is driving the research towards the *transfer* option. In this approach the absorber material (or alternatively the entire device once processed on the primary substrate) must be removed from the primary substrate without damage and ensuring that no rests of the substrate material remain on the absorber's rear surface. These two points are of importance, as they will determine the performance of the final device.

A number of techniques have been proposed in order to establish a clean lift-off process. In general terms they can be classified in two categories, depending on the nature of the actual lifting process:

- The *chemical* approach makes use of an intermediate layer deposited, either between the primary substrate and the active layer, or between the primary

and the alternative substrate (the latter also referred to as the carrier layer), prior to the absorber deposition process. The intermediate layer is removed after processing by dissolving it with a chemical agent. Konagai *et al.*[214] reported on "peeled film technology" already in 1978, by means of a hydrofluoric (HF) solution acting on a sacrificial layer of III-V semiconductor for separating a device from its substrate. Subsequent improvements led to the so-called *epitaxial lift-off* (ELO) process, where a thin epitaxial intermediate layer, typically of AlAs, is selectively etched away by HF, without damage to the GaAs-related active layer[215]. Once lifted off, the active layer can be bonded to a variety of foreign substrates by Van der Waals interactions[216]. The method has been further applied to single and tandem solar cells based on GaInP and GaInP/GaAs, with AlAs as sacrificial layer, by dipping the entire device in the HF solution[217]. Special protecting coating of Cu and plastic film is required in this case on the AlInP window layer, which is easily eroded by the acidic solution. No significant degradation of device performance was found in the single junction reported in [217] when comparing cells on primary substrates and after the ELO process (the last ones reaching efficiencies of 7.97 %), although most authors have reported a reduced power output of ELO-based solar cells. This power reduction has its origin in poor fill factor values, assumed to be a result of an increased series resistance and a high recombination rate associated to the non-alloyed back contact[218]. Furthermore, the formation of microfractures as result of tensile stress, e. g. in the surroundings of point defects or at pinholes, which may enhance leakage currents with a low shunt resistance, cannot be excluded. Further refinements, like those introduced in the *weight-induced* ELO[219], have been carried out towards the optimisation of the lift-off process for large areas, a critical aspect for large-scale applications. Also in the field of optoelectronics, the ELO process has found applications, like the transplantation of light emitting diodes, laser diodes, photodetectors, integrated circuits and quantum well structures based on III-V and II-VI materials onto foreign substrates (see Refs. [220,221] and references therein).
The use of hazardous etching agents clearly complicates the handling of the samples during the chemical lift-off process. Not only careful manipulation is required if the process is not automated, but also additional steps must be taken during the processing, in order to provide protecting coatings on sensitive parts of the device, like buffer or window layers. A convenient alternative would therefore replace aggressive chemicals with harmless solvents. Tiwari and co-workers[222] have developed this technique using NaCl as intermediate layer, which is dissolved in water after processing, demonstrating its applicability to CIGSe-[223] and CdTe-based[224] solar cells with efficiencies of 12.8 % and 11 %[225], respectively.

- The *mechanical* approach takes advantage of an intermediate layer between the primary substrate and the active layer, that detaches under tensile or cleaving stress. A typical procedure was reported by Milnes[226], where a thin soft semiconductor, like Te, is grown epitaxially as the sacrificial layer between the thin-film of interest (e. g. CdTe) and the primary substrate. The application of a strain to the heterostructure results in the fracture along the plane of the sacrificial layer, peeling the thin-film off from the substrate. Of special interest in this approach are layered compounds, since the cleavage is particularly easy in these materials along the van der Waals planes, as

reviewed in Chapter 3. It is well known that an optimal cleavage of layered compounds like WS_2, WSe_2, MoS_2 and $MoSe_2$ can be performed by simply attaching and detaching a piece of scotch tape to the given sample[152].
Finally, laser-based lift-off processes have also been developed for the selective ablation of materials from primary substrates, mainly in the field of optoelectronic devices (see e.g. [227] and references therein).

Despite of the actual peeling process, both the chemical and the mechanical lift-off approaches present common features regarding sample preparation. In particular, the deposition of an intermediate sacrificial layer is compulsory in all cases (except for laser ablation), a step which requires either different deposition parameters from those optimised for the growth of the active layer in the processing chamber, or even the *ex-situ* preparation of the sacrificial layer. This requirement increases the total number of processing steps and the total processing time, an issue to be considered when designing cost-efficient strategies for device implementation.

The results presented in Chapter 3 on the simultaneous formation of a layered chalcogenide film between the rear contact and the absorber layer during the CVD-growth of CGSe thin films suggest a new approach to the lift-off process[228], which can be readily applied to these samples directly after the deposition process. Furthermore, no additional step is required in order to provide the sacrificial layer, as long as the $MoSe_2$ layer playing that role develops itself during the process. Indeed, the characteristic morphology, as revealed by TEM and XRD analysis in Chapter 3, of the layers forming the $MoSe_2$ is nearly ideal for easily lifting the absorber layer off mechanically from its original Mo-coated glass substrate. The existence of domains of type II orientation right at the interface with the CGSe layer corresponds to weakly bonded contact areas by van der Waals interactions between the top chalcogenide and the rear chalcopyrite surfaces, whereas domains of type I orientation still provide a satisfactory adhesion between the layers via covalent bondings. The lift-off process will thus be controlled by the ratio of domain areas of types I and II, as will be discussed in Section 5.3.

Lift-off of CVD-grown CGSe films opens new perspectives for further device processing, regarding on one hand the use of alternative substrates, as mentioned before, and on the other hand the short-term goal of building tandem devices based on chalcopyrite absorbers[229]. The implementation of tandem devices can be realised by the sequential stacking of layers, starting with the high-bandgap absorber CGSe, following with the buffers and low bandgap absorber (e. g. $CuInSe_2$) and the final provision of a metal electrode, to act as rear contact. Once the stacking sequence is completed, the entire structure can be lifted off from the rear CGSe surface and the final steps (buffer, window and front contact provision) processed up-side down on the free CGSe surface.

Of particular interest for the present study of the structural and electronic characterisation of devices based on CVD-grown CGSe is the possibility of accessing directly the rear-interface region of the absorber film for its study. In the following, details on the sample preparation for the lift-off process will be given (Section 5.1). KPFM and XPS/UPS studies performed on the surfaces involved in the lift-off process will be presented in Section 5.2, in order to assess the cleanness of the process. Finally, preliminary results on the characterisation of devices processed on flexible metal substrates will be discussed in Section 5.3.

5.1 Sample preparation

Mechanical lift-off has been successfully performed on CGSe films grown on Mo-coated glass substrates by CVD, as described in Chapter 3, by attaching and detaching stripes of scotch tape on the CGSe top surface in laboratory conditions. This simple procedure provides large peeled-off areas, specially convenient for film characterisation techniques which do not require any rear metal contact, e. g. in Electron Paramagnetic Resonance (EPR)[230]. For the electrical characterisation of films, as well as for the implementation of devices on alternative substrates, the deposition of a metallic rear contact on the top CGSe surface is required prior to proceeding with the lift-off process. The contact can be provided by evaporation or sputtering of a Mo layer, in the same way as the coating of the glass used as primary substrate. The following points outline the standard procedure adopted in this work for the sample preparation of CGSe films prior to the lift-off process:

- Preparation of CGSe samples in the open-tube CVD reactor following a standard single- or two-stage process (see Chapter 3 and Appendix I) on Mo-coated soda-lime glass (SLG). The sacrificial $MoSe_2$ layer grows during the process as an interfacial layer.
- Sputtering of 1 μm thick Mo layer on the CGSe-top surface. This metallic layer provides a good electrical contact and satisfactory adhesion to the alternative substrate and furthermore, it prevents possible damage of the absorber layer during subsequent processing. Figure 87 shows a SEM picture of a sample cross-section after completion of top-Mo coating step.
- Fixing the alternative substrate (a metal foil or, e.g., a second Mo-coated glass substrate for surface characterisation) on the sputtered top Mo layer by means of conductive epoxy, as schematically shown in Figure 88.
- Baking the samples in the oven at 110°C for 45 minutes for cementing the glue.

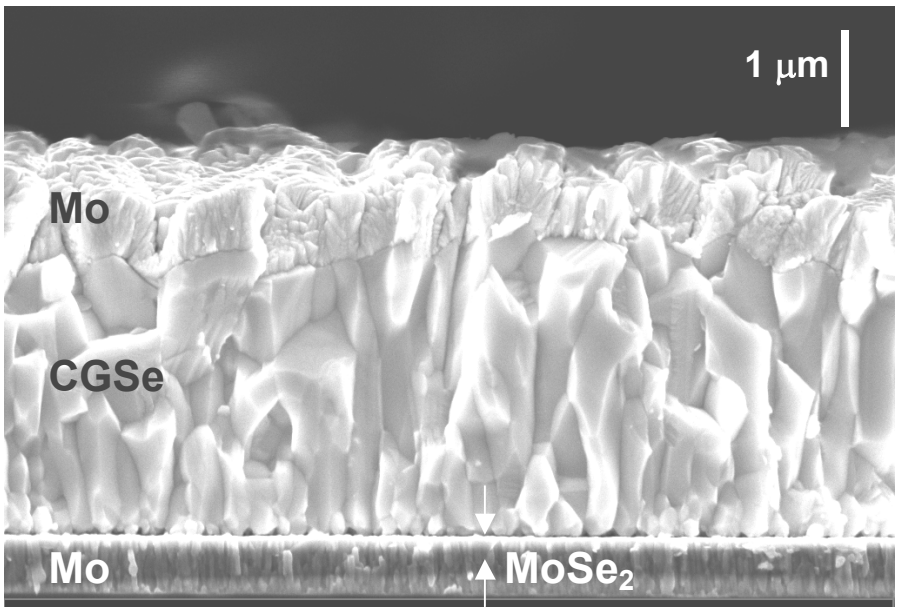

Figure 87. SEM cross-section of a CGSe sample prepared for lifting off from the substrate. A 1 μm thick Mo layer has been sputtered on the top CGSe surface.

Once the sample has been cooled down, the lift-off proceeds by applying a tensile strain on the alternative substrate while holding the primary substrate tight, e. g. with a pair of tweezers, as shown schematically in Figure 88. The heterostructure separates itself from the primary substrate at that location where the weakest interaction between layers exists, i.e. at the interface governed by weak van der Waals forces between the top $MoSe_2$ and the rear CGSe surfaces. As result of the lift-off process, two samples are now available for processing and characterisation: a $MoSe_2$ film on Mo-coated glass and a CGSe/Mo junction on an alternative substrate. The utility of the process will be determined by its cleanness; in other words, if the lift-off process can provide a clean CGSe surface with no remnants of Mo on it (and additionally, a clean $MoSe_2$ surface, with no rests of Cu nor Ga from the absorber layer). The first aspect is crucial for device processing, as the presence of metallic species right at what will be the active p-n junction after the deposition of the buffer and window layers, ruins the formation of the space-charge region at the heterojunction. It will be shown in the coming section that the mechanical lift-off process described above does provide a clean CGSe rear surface, susceptible of further processing and/or characterisation. The second aspect of a clean $MoSe_2$ surface from the lift-off process is only critical with respect to its characterisation, as it constitutes the sacrificial layer for the process.

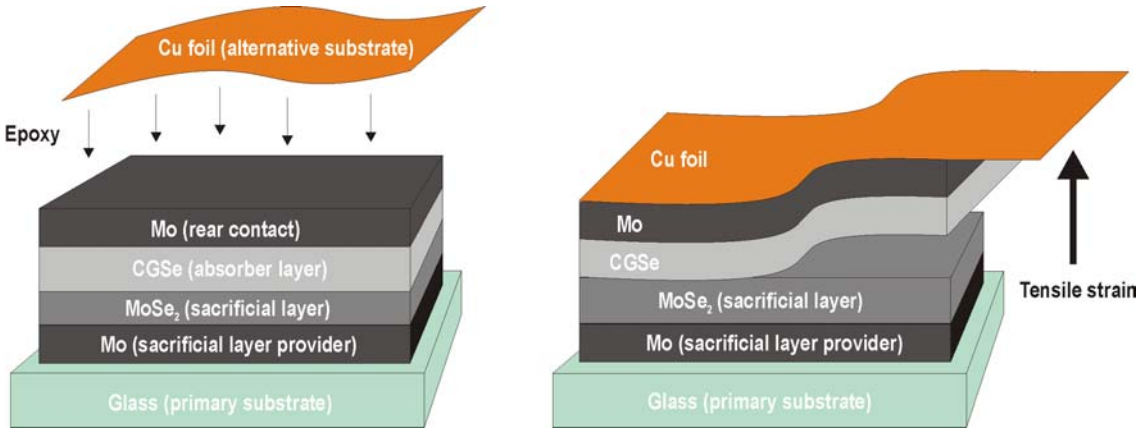

Figure 88. Schematic view of the mechanical lift-off process to transfer the thin-film CGSe active layer to a flexible Cu foil.

5.2 Characterisation of the CGSe/Mo interface

The lift-off process has also been performed under inert-gas atmosphere in a glove-box and in ultra-high vacuum in the preparation chamber of the KPFM system, to ensure contamination-free conditions for the characterisation of the CGSe and $MoSe_2$ surfaces. Kelvin probe force microscopy and photoelectron emission spectroscopy have been used to assess the properties of the as-lifted interface, preserving the surfaces against air oxidation, water vapour and carbon dioxide adsorption.

The procedure stated in Section 5.1 was adapted for the realisation of the lift-off process in UHV, to overcome eventual difficulties in the sample handling. Two pieces from the same sample were coated with sputtered-Mo and provided with a carrier substrate (in this case, a rigid Mo-coated glass substrate for convenience in sample manipulation). The samples were mounted on the sample holder of the microscope, on the primary substrate in one case and upside-down on the carrier substrate in the other, to expose both the $MoSe_2$ and the CGSe surfaces after the lift-off to the scanning tip. Both samples were introduced in the entrance chamber of the KPFM system, subsequently evacuated to UHV ($p<10^{-10}$ mbar), and annealed at 110°C for 45 minutes to desorb water vapour prior to their transfer into the preparation chamber. The lift-off was then performed in UHV with the help of the manipulator, tearing in one case the carrier substrate off, as depicted in Figure 88, for the $MoSe_2$ characterisation, and the primary substrate in the second (upside-down) case for the CGSe characterisation. KPFM measurements were performed on both samples, which were subsequently transferred to a portable sample-transfer-unit and carried to the XPS-system. The transfer unit was provided with a battery and a turbo-pump with an autonomy of 12 hours, able to keep the samples under high vacuum conditions ($p<10^{-8}$ bar) during the sample transport. The experiment was completed with photoelectron emission analysis on the samples under study. In parallel, CGSe samples grown in the same two-stage run as those used for the interface study were processed as standard solar cells to assess the sample quality, showing efficiencies of 6.8 % and open-circuit voltages above 800 mV.

This procedure permits the realisation of KPFM and XPS measurements of the CGSe/$MoSe_2$ interface under optimal cleanness conditions. This issue is of critical importance, as both techniques are extremely surface-sensitive. Additional XPS measurements were carried out after lifting samples off from the original substrates in a glove-box under 1 bar N_2 atmosphere. The glove-box was connected to the XPS system via a preparation chamber, ensuring that samples to be measured were not exposed to air. Reproducible XPS results were found from both types of lift-off samples, either prepared in high-vacuum or under inert-gas atmosphere. Due to constraints in the sample manipulation under UHV, only small areas in the range of 0.5 mm^2 could be prepared for the subsequent analysis. In order to avoid overlapping signals from the Mo-containing substrate on the CGSe rear side spectra, the spot size of the X-ray source had to be adjusted, resulting in a poor signal-to-noise-ratio for reasonable measuring times. XPS/UPS results presented in Section 5.3.3 will thus refer for the sake of clarity to the case of samples prepared under inert gas atmosphere, as larger areas and improved signal-to-noise ratio could be obtained from them.

5.2.1 The $MoSe_2$ surface

The topography of the $MoSe_2$ top surface as measured with the KPFM is shown in Figure 89. Planar domains are visible over large areas of about 400x200 nm^2 which are attributed to domains of type-II orientation. Terrace-like edges are discernible at some of these plateaus, consisting of steps of tens of nm formed by a few chalcogenide layers each. Emerging among these flat regions, additional extrusion-like protuberances appear, which account for much of the total surface roughness. These protuberances are narrow, in the order of 150x50 nm^2, and apparently disposed with a common orientation but otherwise randomly distributed over the entire scanned surface. These regions are

attributed to domains of type-I orientation, i.e. these are the regions providing intimate contact between the chalcogenide and the chalcopyrite layers.

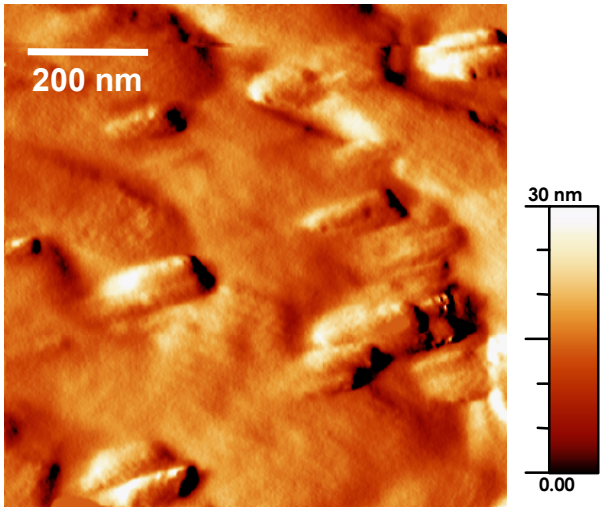

Figure 89. Topography of the $MoSe_2$ top surface after lift-off in UHV, as measured with KPFM.

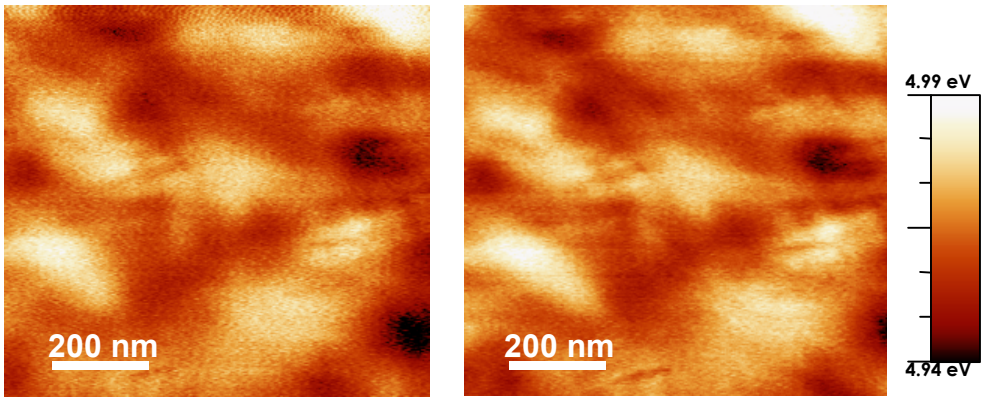

Figure 90. (Left) Work function mappings of the $MoSe_2$ top surface after lift-off in UHV in darkness and **(right)** under illumination (λ=442 nm, p~60 mW).

Measurements of the contact potential on the $MoSe_2$ top surface in darkness and under illumination show fairly constant work function values, comprised between 4.94 eV and 4.99 eV, and minor surface photovoltage, as shown in Figure 90 over the same position of Figure 89. No evident correspondence between the topography and variations in the work function mapping is found, except for some of those areas where protuberances show up, which is understood as resulting from slight variations of the local doping concentration, rather than corresponding to different facets of $MoSe_2$ domains.

5.2.2 The $CuGaSe_2$ rear surface

Figure 91 shows SEM and KPFM images of the UHV-lifted-off CGSe rear surface topography, from the same sample as that shown in Figure 87. A granular texture is visible in both images, corresponding to the base of the columnar grains visible in Figure 87, with lateral dimensions of single grains between 50 nm and 400 nm size. Local domains of irregularities at the apex of some grains are visible in the KPFM topography, presumably corresponding to the contact areas between the absorber layer and the $MoSe_2$. The morphology of the layer differs from those lift-off samples of Ga-rich compositions shown in Figure 43, corresponding in this case to Cu-rich morphologies, characteristic of the two-stage process, as discussed in Chapter 3.

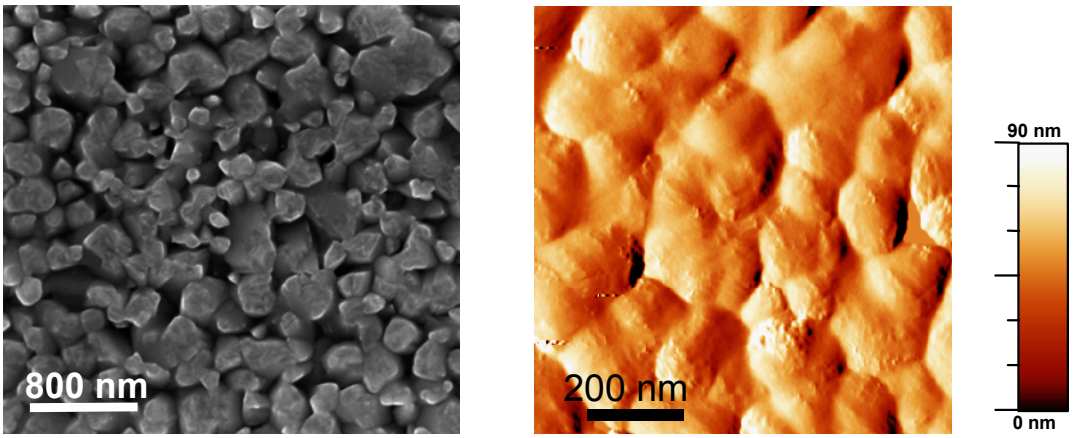

Figure 91. (Left) SEM image of the CGSe rear surface. **(Right)** Topography image obtained by KPFM of the same sample. The lift-off process was performed under UHV conditions.

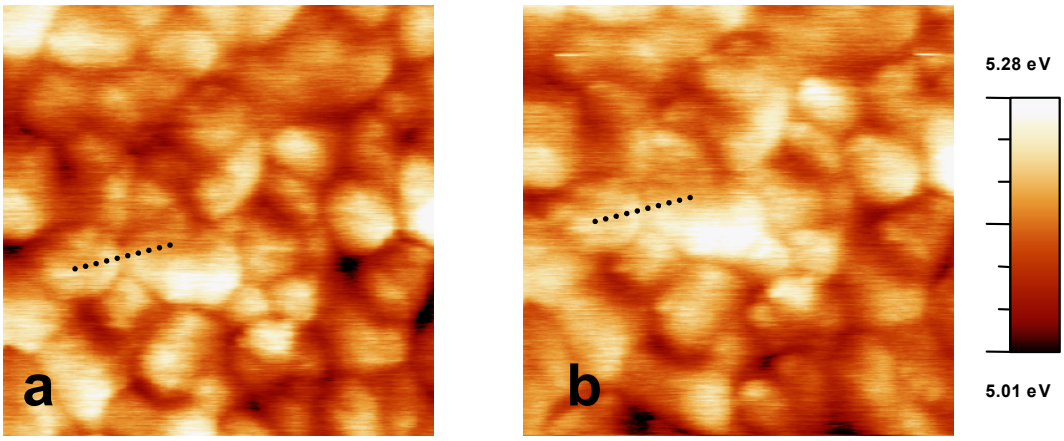

Figure 92. Work function images obtained by KPFM of the rear CGSe surface after lift-off in UHV, in darkness **(left)** and under illumination with HeCd laser (20 mW, λ = 675 nm) **(right)**. A slight shift in the –y direction between both measurements can be appreciated. The dotted line corresponds to the line-scan shown in Figure 93.

Contact potential measurements in the dark were recorded simultaneously on the same position of the rear CGSe side where the topography image was obtained. The mapping, showing absolute work function values, after calibrating the tip against the reference HOPG sample, is shown in Figure 92 (left). Grain boundaries can be identified by direct inspection and comparison to the topographical image, showing lower work function values than the inner parts of the crystallites. A work function line-scan taken along the dotted line indicated in Figure 92 is shown in Figure 93 as an example. The average work function lowering $\Delta\Phi$ at grain boundaries, after performing a number of line-scans at different positions, was found to be 50 ± 10 meV, the drop extending over a range of about 100 nm. The $\Delta\Phi$ value is slightly lower than that reported from KPFM measurements on the top surface of PVD-grown CGSe samples briefly exposed to air[231]. Contrarily to the case of Cu-rich compositions shown in Chapter 3, where secondary phases were identified as segregations along grain boundaries, the Ga-rich composition characteristic of the two-stage growth results in a downward band bending at boundaries between CGSe crystallites. This is a common feature found in a variety of p-type chalcopyrite absorber layers[231], where holes act as majority carriers, facing potential barriers at grain boundaries.

Illuminating the sample with red light (λ = 675 nm), as shown in Figure 92 (right) results in an overall increase of the work function of 80 ± 15 meV, attributed to the flattening of the surface band bending, in agreement with the results presented in Chapter 3 on cross-sections. A slight reduction of the potential barrier at grain boundaries is recorded under illumination, with an average value of 45 ± 10 meV. The decrease of the potential barrier by optical excitation can be understood as the result of photogenerated minority carriers being trapped at ionised donor-like interface states associated to the grain boundary, thus passivating to some extent the interface.

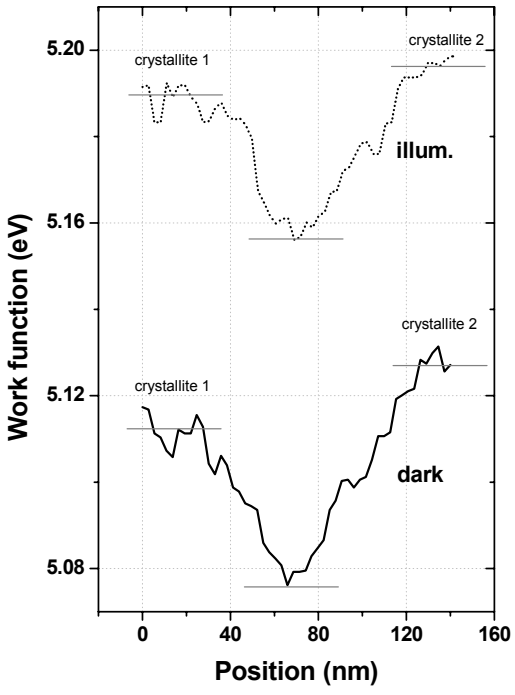

Figure 93. Work function drop at a grain boundary between two CGSe crystallites, corresponding to the dotted lines in Figure 92, in darkness and under illumination.

A quantitative analysis of grain boundary properties can be performed according to the model developed by Seto[232], for the case of moderate doping concentration of the crystallites. The space-charge region extending into the bulk of each crystallite is small in comparison to the crystallite size, according to Figure 92, and therefore the equations derived for the built-in potential as a function of the doping concentration in a depletion region also apply. From Eq. 16 it follows:

$$\frac{\Delta\Phi_b}{q} = \frac{qN_A w^2}{2\varepsilon\varepsilon_o} \qquad \text{Eq. 122}$$

where $\Delta\Phi_b/q$ is the potential drop across the grain boundary. Substituting the values for $\Delta\Phi_b$, the depletion width w, and assuming[148] $\varepsilon\sim10$ for CGSe, a net doping concentration in the crystallites of $2.4\cdot10^{16}$ cm^{-3} is found, in excellent agreement with the results presented in Eq. 116. The depletion region associated to the grain boundary builds up as a result of charge storage of opposite sign at interface states. The density of charged states located at the boundary N_{gb} can thus be calculated from the previous values of voltage drop and net doping, according to:

$$\Delta\Phi_b = \frac{qN_{gb}^{\ 2}}{8\varepsilon\varepsilon_o N_A} \qquad \text{Eq. 123}$$

From this expression, $N_{gb} = 2.4\cdot10^{11}$ cm^{-2} in darkness, decreasing slightly down to $2.2\cdot10^{11}$ cm^{-2} under illumination, confirming the reduction of the positive stored charge by means of photogenerated carriers. Detailed studies of the electronic transport across grain boundaries in PVD-grown CGSe performed by Schuler[66] led to the conclusion that ionised donor-like defects in concentrations of the range of $1\cdot10^{12}$ cm^{-2} are located at grain boundaries, in good agreement with the present results.

The potential barrier for the hole transport measured at grain boundaries, amounting to ~50 meV, is significantly lower than the activation energy obtained for the series resistance from the dark J(V, T) analysis in Section 4.3. It is therefore concluded that the origin of the 0.3 eV potential barrier for the hole transport in the valence band, as inferred from the analysis, is not related to grain boundaries, thus supporting the model presented in Chapter 4 for the blocking behaviour via the mediation of the interfacial $MoSe_2$ layer at the back contact.

5.2.3 Characterisation with photoemission spectroscopy

Photoemission experiments (XPS and UPS) were performed on the samples after completion of the KPFM studies in order to assess the cleanness of the lift-off process. The samples were transferred in high-vacuum, as mentioned above, to avoid surface contamination. Additional samples were prepared in the glove box connected to the XPS system under inert gas atmosphere to provide larger lift-off areas for the analysis. Reproducible results were found in both cases, with an improved spectra quality due to a higher count rate in the case of samples prepared under inert gas atmosphere. Overview spectra of the latter samples, from both surfaces, obtained in normal emission

using Mg K_α radiation as excitation source at a base pressure of $8 \cdot 10^{-10}$ mbar, are shown in Figure 94. The $MoSe_2$ surface appears clean, with minor traces of oxygen and carbon, as indicated by the dotted lines over the spectra. No remnants of copper nor gallium were found on the chalcogenide surface, comparing to the characteristic emissions from CGSe. No traces of Mo (inferred from the Mo 3p, Mo 4s and Mo 4p signals, as the most prominent Mo 3d overlaps with the Se 3s emission) are found on the CGSe rear side, thus demonstrating the suitability of the lift-off approach proposed in Section 5.1 for separating the active layer from the primary substrate. Additionally, significant amounts of carbon and oxygen are found on the CGSe rear side, whose presence is attributed to contaminants from the Mo-coating prior to the CVD deposition process. The uneven distribution of contaminants between the $MoSe_2$ and the CGSe surfaces is attributed to their different reactivities, in particular to the inertness of van der Waals planes over large domains of type II orientation of the $MoSe_2$, identified in Figure 89.

UPS spectra of both samples were obtained using He I (21.22 eV) excitation source. The valence band edges measured from the CGSe rear side and the $MoSe_2$ top surface are shown in Figure 95. The energy difference between the Fermi level (zero in the abscissa, as calibrated with a sputter-cleaned Au foil reference) and the uppermost valence band edge was calculated by the linear extrapolation of the leading edge over the background level, indicated by solid lines in the figure. The obtained values, E_F-E_V=0.5±0.1 eV for CGSe and E_F-E_V=0.2±0.1 eV for $MoSe_2$, would result in a valence band offset ΔE_V~0.3 eV when bringing both materials in intimate contact during the heterojunction formation, neglecting element intermixing (in agreement with the XPS overview spectra), the band bending associated to the junction formation, and the effects of surface dipoles.

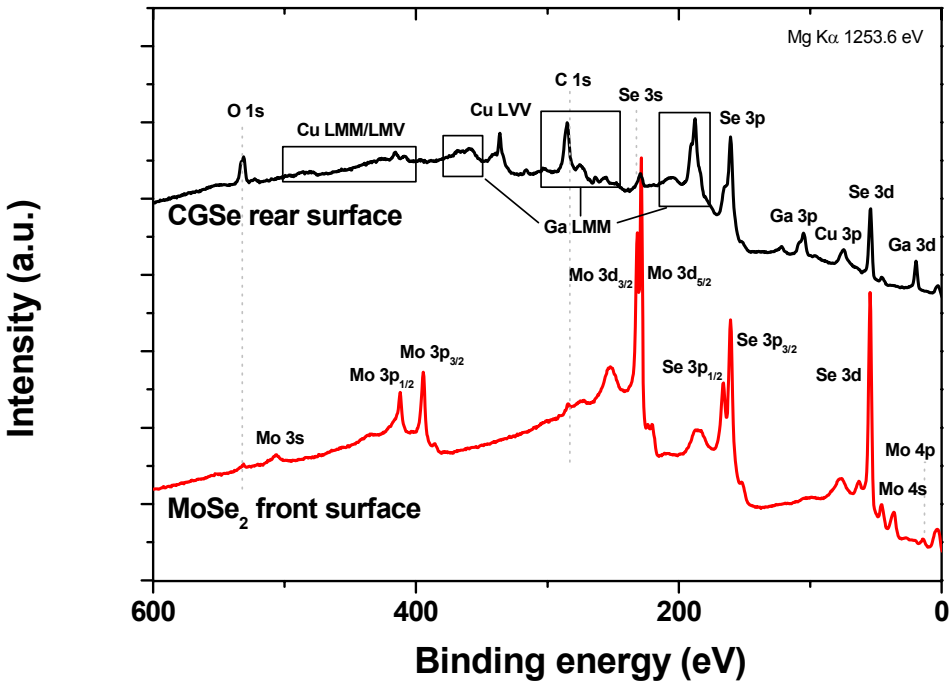

Figure 94. XPS overview spectra of lift-off samples under inert atmosphere: CGSe rear surface (upper) and $MoSe_2$ top surface (lower). Mg Kα (1253.6 eV) was used as excitation source, with 20 eV pass energy.

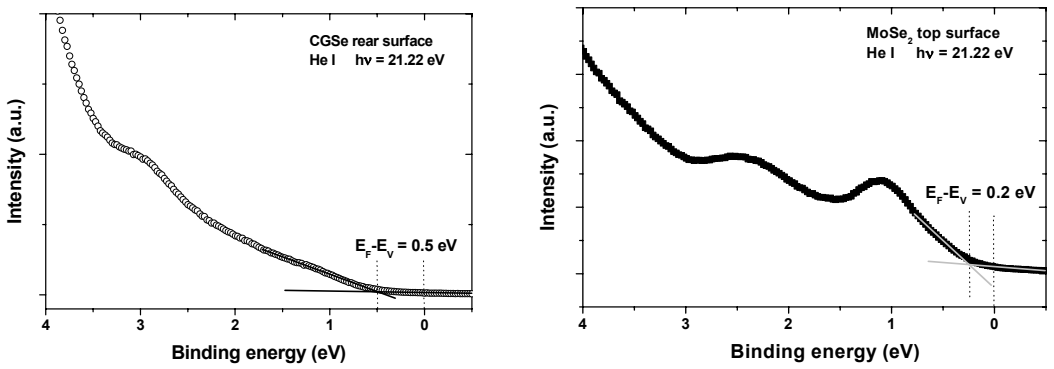

Figure 95. UPS spectra of the valence band edges of CGSe and $MoSe_2$, after lift-off under inert atmosphere. He I (21.22 eV) was used as excitation source. Positions in energy scale of valence band edges are included referred to the Fermi level.

The value of the valence band offset inferred from the photoemission study of the lift-off interfaces, under the mentioned assumptions, is in excellent agreement with the energy band diagram proposed in Chapter 4 on the basis of the current-voltage analysis of CGSe-based devices, and it is thus interpreted as a supporting argument for the validity of the model.

5.3 Solar cells on alternative substrates

The lift-off process allows implementing thin-film solar cells on foreign substrates, e.g. flexible metal or plastic foils, which can otherwise suffer severe degradation during the absorber film processing under the reactive atmosphere in the CVD process. Solar cells, like the one shown in Figure 96, have been processed from two-stage grown CGSe absorbers within the frame of this work on Cu foils, following the procedure stated in Section 5.1. Once the lift-off has been performed, the sample is provided with a standard CdS buffer layer by CBD and a sputtered ZnO window, as explained in Chapter 1. Ni-Al front contacts are subsequently evaporated.

The electronic characterisation of lift-off devices was carried out by means of quantum efficiency and J-V analyses. Figure 97 shows the external quantum efficiency of a lift-off device of 0.5 cm^2 area based on a two-stage grown CGSe absorber at room temperature without applied bias. Significant losses are readily seen in the long wavelength range, indicating a reduced collection efficiency, when comparing this plot to the corresponding normalised quantum efficiency of two-stage based devices on conventional Mo-coated glass substrates from the same absorber growth process. Indeed, reasonable yields, comparable to those cases of devices processed on single-stage grown absorbers, are found in the medium wavelength range, showing values above 0.7 around 575 nm, which indicates that only those carriers generated in the vicinity of the junction can be effectively collected.

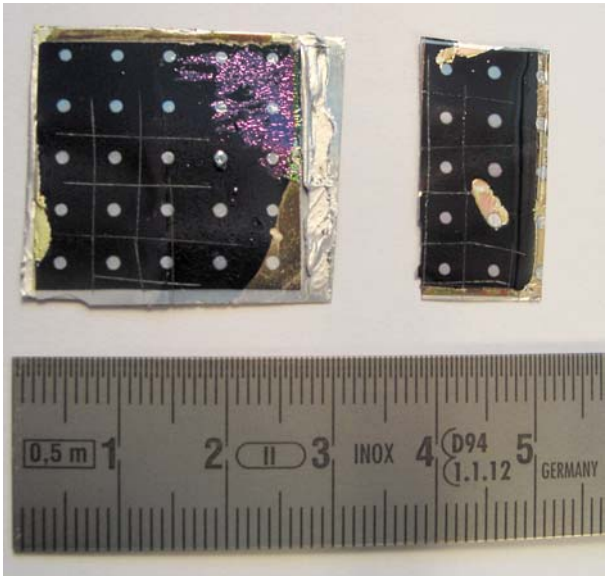

Figure 96. Thin-film solar cells based on CVD-CGSe, processed on the rear side after lifting the absorber film off from the original Mo-coated glass substrate. Flexible Cu foils were used as alternative substrates, fixed with conductive epoxy on the previously Mo-sputtered top surface of the CGSe sample, as explained in Section 5.1.

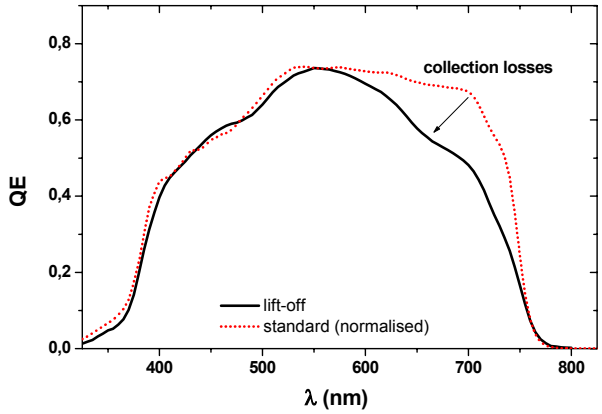

Figure 97. External QE without applied bias (solid line) of a lift-off CGSe-based solar cell. As comparison, the QE (normalised to the maximum value of the lift-off yield) of a conventional device based on a two-stage absorber from the same process is included. The yield is affected by a steep decrease in the long wavelength range, indicating severe collection losses.

Figure 98 shows the J(V, T) characteristics under illumination of a lift-off solar cell of 15 mm^2 area based on a two-stage grown CGSe absorber, and the corresponding temperature dependence of the open-circuit voltage V_{oc}. The device performance of lift-off devices is characterised by poor V_{oc} and FF values, resulting in efficiencies below 1 % under standard AM1.5G conditions[1]. This fact points to low values of the shunt

[1] Highest PV parameter values under AM1.5G at room temperature are: V_{oc} = 240 mV, J_{sc} = 9.8 mA/cm^2, FF = 0.27, and η = 0.6 % from a 0.5 cm^2 total area device.

resistance, with leakage currents dominating the electronic transport. Low extrapolated V_{oc} values at T=0K, slightly above 600 mV as shown in Figure 98, confirm the poor performance of the p-n junction in controlling the electronic transport of lift-off devices.

Thermographical analyses, based on the detection of uneven infrared emissions resulting from temperature gradients in the samples under study[233], have demonstrated the impact of shunt paths on lift-off samples under operation conditions. Figure 99 shows a thermography overlapping an optical image of one of such devices under short-circuit conditions. The active solar cell is delimited in the figure by a rectangular scrape, on which the front contact grid is visible with darker contrast. The front electrode probe is visible as a tip on the left part of the image. A second probe (not visible) on the rear contact closes the circuit. Bright-contrast regions correspond to those areas where heat is being dissipated, which are found to correspond to the scribing edges delimiting the cell. The local heat release takes place in those regions of the cell affected by shunt paths, resulting in leakage currents and the dissipation of the obtainable power output from those other regions of the cell showing a satisfactory performance (indeed, most of the active area, as concluded from Figure 99).

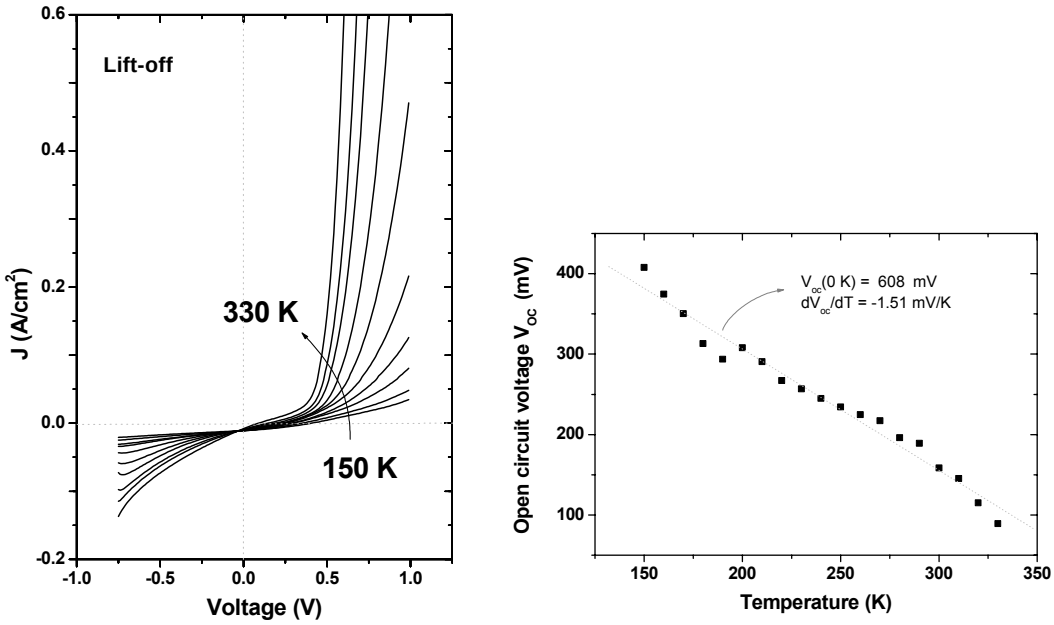

Figure 98. (Left) J(V, T) characteristics under AM1.5 conditions of a lift-off sample processed on a flexible Cu-foil. **(Right)** Open-circuit voltage V_{oc} as a function of the temperature, with the extrapolated value at 0K and the variation rate.

Finally, it should be mentioned that no blocking behaviour is inferred at low temperatures from the illuminated J(V,T) curves shown in Figure 98 in lift-off devices. This observation is in agreement with the model presented in Chapter 4 on the role played by the interfacial $MoSe_2$ in the observed effect as mediator of the rear contact, as the $MoSe_2$ layer is removed from the absorber rear surface during the lift-off process.

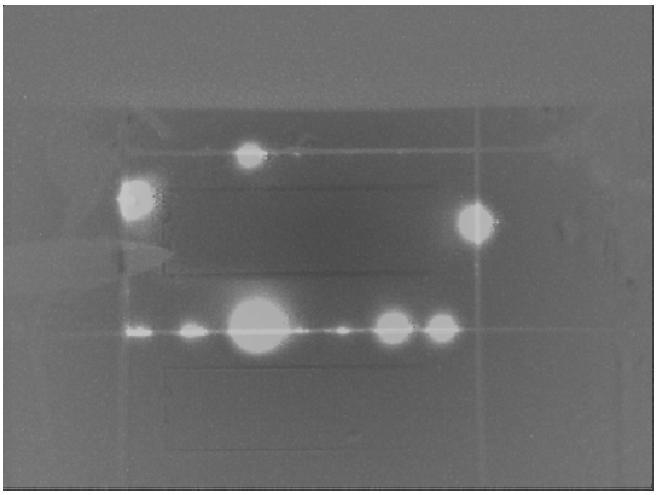

Figure 99. Thermography of a lift-off CGSe solar cell processed on a Cu-foil, overlapping an optical image on the same position. Bright-contrast regions correspond to local heat release, due to power dissipation in shunts, which appear along the scrape delimiting the cell borders.

It is thus concluded that the optimisation of cell processing, and particularly the cell scribing, after the realisation of the lift-off process following the approach proposed in Section 5.1, is thus necessary in order to obtain acceptable output figures from this type of devices.

5.4 Chapter summary

A new approach to the lift-off process, a field of increasing relevance in optoelectronics and thin-film photovoltaics, has been proposed and assessed in this chapter.

On the basis of the results presented in Chapter 3, regarding the formation and structural characterisation of an intermediate $MoSe_2$ layer during the growth of CGSe thin films by CVD, a simple lift-off procedure for the removal of the active CGSe films from the original substrates on which they are grown has been stated. This method presents some advantages with respect to alternative approaches reported in the literature. In particular, the simultaneous formation of the sacrificial layer during the growth of the absorber film simplifies the process, reducing the number of processing steps and the processing time, an issue of interest for eventual applications.

For the first time, data on the structural and electronic properties of the rear side of CGSe thin films have been reported. Surface-sensitive techniques KPFM and XPS/UPS have been used for the characterisation of the free surfaces after lifting the CGSe absorber film off from the primary substrate, in UHV and under inert gas atmosphere. The analysis of potential barriers at CGSe grain boundaries have led to estimations of the CGSe net doping concentration ($2.4 \cdot 10^{16}$ cm^{-3}) and of the density of interface states associated to grain boundaries ($2.4 \cdot 10^{11}$ cm^{-2}) in good agreement with results from the literature and the studies on cross-sections presented in Section 3.4.

The surface cleanness after the lift-off process, of crucial importance for further device processing, has been assessed by means of KPFM and XPS/UPS, revealing that the mechanical lift-off takes place right at the interface between the CGSe absorber and the interfacial $MoSe_2$. No remnants of Mo were found on the CGSe rear surface, neither Cu nor Ga rests on the $MoSe_2$ top surface, as concluded from experiments conducted in UHV and under inert gas atmosphere. Typical contaminants, namely oxygen and carbon, were however found on the CGSe rear surface, whose origin was attributed to contamination of the primary Mo-coated substrate prior to CVD processing.

Preliminary results on the characterisation of devices processed from lift-off samples have been presented and major limiting factors affecting their performance have been identified. Leakage currents, mainly related to edge effects of the cell scribing, limit the collection efficiency of the heterojunction, resulting in poor fill factor, open-circuit voltage and efficiency figures. Optimisation of the post-lift-off device processing is thus required, in order to apply the method e.g. to the implementation of tandem devices in combination with low band gap absorbers.

Finally, further hints supporting the band diagram model presented in Chapter 4, regarding the mediation of the interfacial $MoSe_2$ layer to the rear contact, and accounting for the blocking behaviour observed in the current-voltage characteristics of standard devices at low temperatures, have been presented. Concretely, an excellent agreement has been found between the valence band offset at the CGSe/$MoSe_2$ inferred from UPS measurements (~0.3 eV) and that included in the band diagram of the heterojunction proposed in Chapter 4 accounting for the activation energy of the apparent series resistance (~0.27 eV). The role of grain boundaries as potential barriers for the hole transport in CGSe, amounting ~50 meV, has been shown not to be sufficient to explain the high activation energies observed. Furthermore, devices processed on lift-off absorbers do not show the characteristic blocking behaviour, which is attributed to the absence of the interfacial $MoSe_2$ layer at the rear contact.